Research Article

An investigation into the adverse effects of O_2, SO_2, and NO_x on polyethyleneimine functional CO_2 adsorbents

Kaimin Li[1] · **Jianguo Jiang**[2]

Received: 5 December 2020 / Accepted: 9 February 2021 / Published online: 18 February 2021

Abstract
In this study, we investigated the influence of O_2, SO_2, and NO_x on branched and linear polyethyleneimine (PEI) functional silica CO_2 adsorbents (BPEI-SiO_2 and LPEI-SiO_2, respectively). O_2 was much more likely to oxidize BPEI-SiO_2, compared with LPEI-SiO_2, to form C=O and C=N groups and led to a 23.0% decrease in the CO_2 adsorption capacity after 990 min of cumulative contact with 10% O_2. In contrast, LPEI-SiO_2 lost only approximately 3.6% of its CO_2 adsorption capacity, although O_2 oxidized LPEI-SiO_2 to form C=O groups. SO_2 can cause severe degradation of BPEI-SiO_2 and LPEI-SiO_2 by forming heat-stable NH_3^+—and/or NH_2^+—containing adducts and by promoting the formation of urea linkages. After cumulative contact with 10, 50, and 200 ppm SO_2 for 990 min, BPEI-SiO_2 lost 18.2%, 61.4%, and 89.0% of its CO_2 adsorption capacity, and LPEI-SiO_2 lost 18.5%, 60.6%, and 78.5% of its CO_2 adsorption capacity, respectively. NO_2 at 10 ppm and NO at 200 ppm caused almost no loss in CO_2 adsorption capacity after cumulative contact for 990 min, but both led to degradation of adsorbents. NO_2 can cause irreversible formation of NH_3^+—and/or NH_2^+—containing adducts, acid products, N-nitro compounds (N–NO_2), C-nitroso compounds (C–N=O), and C-nitro (C–NO_2) compounds, and can promote the formation of urea linkages. NO can lead to the formation of NH_3^+—and/or NH_2^+—containing adducts and N-nitroso (N–N = O) compounds.

Keywords Carbon capture · Chemical degradation · Flue gas · Polyethyleneimine · Solid amine adsorbents

1 Introduction

CO_2 capture, utilization, and storage is a critical technology for realizing net-zero emissions [1]. Over the past decades, CO_2 adsorbents, such as zeolite [2, 3], porous carbon [4, 5], metal–organic frameworks [6, 7], calcium looping technology [8, 9], and solid amine adsorbents [10–12], have attracted much attention for capturing CO_2 from flue gas. Of the various adsorbents, solid amine has been considered a good choice for trapping CO_2 directly from flue gas due to its excellent CO_2 adsorption performance and low energy penalty [13–16]. To protect solid amine adsorbents from high concentrations of SO_2 (500–2500 ppm) and NO_x (1500–2500 ppm) [17–24] during post-combustion CO_2 capture, the best location of the CO_2 capture unit is after flue gas denitrification and desulfurization [23, 25–27]. However, a certain amount of SO_2 (50–200 ppm), NO_x (100–400 ppm) [16, 27–32], and O_2 (3–10%) [21, 33–36], which can cause degradation of solid amine sorbents, are still present in the flue gas after denitrification and desulfurization.

According to previous studies, O_2 can oxidize the organic components of solid amine sorbents by forming C=O [21, 37–42], N=O [40–42], C=N [37, 40, 42, 43],

Supplementary Information The online version contains supplementary material available at https://doi.org/10.1007/s42452-021-04352-7.

✉ Kaimin Li, likaimin16@gmail.com; ✉ Jianguo Jiang, jianguoj@tsinghua.edu.cn | [1]Department of Civil and Environmental Engineering, The Hong Kong Polytechnic University, Hong Kong, China. [2]School of Environment, Tsinghua University, Beijing 100084, China.

and aliphatic C=C/heterocyclic C-N/aromatic C=C [23]. Furthermore, SO_2 can lead to degradation of solid amine adsorbents by forming sulfate [17, 22, 44], sulfite [17, 22, 44, 45], bisulfite (under humid conditions) [45], and even nitro- and quinone-type compounds (aromatic amine) [22]. NO_2 can result in degradation of solid amine adsorbents by forming nitrate and nitro-compounds [46, 47]. Although it has been reported that NO has no apparent adverse effects on solid amine sorbents [27, 31, 44, 46, 48, 49], a few researchers found that NO can lead to the loss of CO_2 adsorption capacity in solid amine sorbents [28, 50].

Overall, the degradation of solid amine adsorbents induced by O_2, SO_2, and NO_x has been investigated relatively comprehensively by past studies. However, there is still a lack of information on the degradation of PEI functional adsorbents when interacting with O_2, SO_2, and NO_x, which is the focus of this study. BPEI and LPEI functional adsorbents were evaluated during long-term interactions with O_2, SO_2, and NO_x. Their degradation mechanisms were explored in more detail to clarify the degradation pathways of PEI molecules.

2 Experimental work

2.1 Chemicals

BPEI (molecular weight [MW] 25,000) and potassium bromide (KBr, IR grade) were purchased from Alfa Aesar (Tewksbury, MA, USA). LPEI (MW 25,000) was purchased from Polysciences (Warrington, PA, USA). The molecular structures of BPEI and LPEI are shown in Scheme S1 in the Supplementary Information. Methanol (HPLC grade) was purchased from Fisher Scientific (Waltham, MA, USA). Nano silica used as support was synthesized in lab, its surface area and pore volume respectively were 418 m^2/g and 0.84 cm^3/g [51]. All of the gases, including 99.999% N_2, 15% CO_2 balanced with N_2, 15% CO_2 and 10% O_2 balanced with N_2, 15% CO_2 and 200 ppm NO balanced with N_2, 15% CO_2 and 10 or 200 ppm NO_2 balanced with N_2, 15% CO_2 and 10, 50, or 200 ppm SO_2 balanced with N_2, were provided by ZG Special Gases (Beijing, China).

2.2 Preparation of PEI functional adsorbents

First, BPEI or LPEI was dissolved into 25 ml methanol and stirred for 30 min using a magnetic mixer. Second, 2 g nano-silica was added to the solution. The silica had been dried in an oven at 105 °C under vacuum conditions (< 1 mm Hg) for 3 h. Third, another 5 ml methanol was added to the solution with stirring at ambient temperature until all of the methanol evaporated. Finally, the sample was dried at 50 °C under vacuum conditions (< 1 mm Hg) for 2 h. The products were named BPEI-SiO_2 and LPEI-SiO_2.

2.3 Characterizations

CO_2 cyclic adsorption–desorption tests were conducted using the TGA/DSC 2 thermogravimetric analyzer (Mettler Toledo, Greifensee, Switzerland). First, 15–20 mg adsorbents were placed into an aluminum oxide pan and pretreated at 120 °C for 30 min under a N_2 atmosphere. Second, the samples were cooled to 75 °C, and the N_2 gas was substituted with gas 1 (15% CO_2 balanced with N_2) for a 10-min adsorption period. The temperature was elevated, and gas 1 was switched to N_2 for 10 min desorption at 120 °C. Third, the samples were cooled to 75 °C, and the gas was switched from N_2 to gas 2 (15% CO_2 with some O_2, NO, NO_2, or SO_2 in N_2) for 10 min adsorption. The temperature was elevated, and gas 2 was switched to N_2 for 10 min desorption at 120 °C. Finally, the second and third steps were repeated 100 times. A reference test was also performed in which the second step was repeated 200 times. At the end of each test, the samples were stabilized for 2 h at 75 °C under a N_2 atmosphere. For the analysis, the CO_2 adsorption capacity of the 1st, 3rd, 5th, …, and 199th cycles were used. The samples used for cyclic adsorption–desorption tests under different conditions were denoted as BPEI-SiO_2 or LPEI-SiO_2, followed by the volumetric concentration of CO_2, O_2, SO_2, or NO_x in brackets. For example, BPEI-SiO_2(200 ppm NO) refers to BPEI-SiO_2 samples exposed to 200 ppm NO (15% CO_2 and 200 ppm NO balanced with N_2) in the adsorption–desorption cycles. BPEI-SiO_2(15% CO_2) or LPEI-SiO_2(15% CO_2) indicate that no O_2, SO_2, or NO_x was present during the adsorption–desorption tests.

Diffuse reflectance infrared Fourier transform (DRIFT) spectra for fresh adsorbents and samples from cyclic adsorption–desorption tests were collected by the Nicolet 6700 spectrometer coupled with an in situ reaction cell (Thermo Fisher Scientific, Waltham, MA, USA). The resolution and scan time were set as 4 cm^{-1} and 32, respectively. The spectra were recorded in the range of 400–4000 cm^{-1}. The spectrum of KBr under N_2 was used as the background. In situ DRIFT spectra of BPEI-SiO_2 and LPEI-SiO_2 during interaction with different gas mixtures were also recorded using the Nicolet 6700 spectrometer. First, fresh samples of BPEI-SiO_2 and LPEI-SiO_2 were placed in the in situ reaction cell, the cell was sealed, and the sample was degassed for 2 h at 120 °C under N_2. The spectra were recorded and denoted as spectrum 1. Second, the samples were cooled to 75 °C under N_2, and the spectra were collected and used as the background for recording the test spectra in the presence of gases 1 or 2. Third, the N_2 was switched to gas 1 or gas 2, and simultaneously start to record infrared

(IR) spectra at certain time points. Finally, after 10 or 24 h of interaction with gas 1 or gas 2, the temperature was increased and the atmosphere simultaneously switched to N_2. Samples were regenerated at 120 °C under N_2 for 1 h, and the IR spectra were recorded (using spectrum 1 as a background).

3 Results and discussion

3.1 The adverse effects of O_2

Figure 1 shows the CO_2 adsorption capacity for BPEI-SiO_2(10% O_2) and LPEI-SiO_2(10% O_2), as well as BPEI-SiO_2(15% CO_2) and LPEI-SiO_2(15% CO_2). BPEI-SiO_2(15% CO_2) and LPEI-SiO_2(15% CO_2) exhibited a relatively stable CO_2 adsorption performance during the tests. However, BPEI-SiO_2(10% O_2) lost 23.0% of its original CO_2 adsorption capacity by the 199th cycle. In contrast, LPEI-SiO_2(10% O_2) displayed almost the same stable performance as LPEI-SiO_2(15% CO_2) and only lost approximately 3.6% of its original CO_2 adsorption capacity by the 199th cycle. The CO_2 cyclic adsorption–desorption results demonstrate that LPEI is much more resistant to oxidation by O_2 than BPEI, which is consistent with previous research [37].

Figure 2a shows the DRIFT spectra of BPEI-SiO_2, BPEI-SiO_2(15% CO_2), and BPEI-SiO_2(10% O_2), and Fig. 2b shows the DRIFT spectra of LPEI-SiO_2, LPEI-SiO_2(15% CO_2), and LPEI-SiO_2(10% O_2). Among the DRIFT spectra of BPEI-SiO_2, BPEI-SiO_2(15% CO_2), and BPEI-SiO_2(10% O_2), the most apparent difference is the peak at 1666 cm^{-1}. The weak peak in the case of BPEI-SiO_2 represents the C=O stretching vibration in carbamate and carbamic acid formed by adsorbing CO_2 from the atmosphere [13, 52–56]. The peak's absorption intensity in BPEI-SiO_2(15% CO_2) is slightly stronger than in BPEI-SiO_2 but weaker than in BPEI-SiO_2(10% O_2), mainly due to the C=O vibration in urea linkages [13, 57]. For BPEI-SiO_2(10% O_2), the peak at 1666 cm^{-1} becomes very prominent and is likely associated with the oxidation of BPEI-SiO_2 by O_2 for various reasons. Bali et al. [38, 45] assigned a similar IR peak, located at 1693 cm^{-1}, as the C=O stretching vibration of amide, acid, and/or imide. Wang et al. [39, 58] assigned a similar band (1659 cm^{-1}) as the amide's C=O stretching vibration. Srikanth et al. [41, 53] assigned a similar peak at 1670 cm^{-1} as the C=O stretching vibration in amide overlapping with the N=O stretching vibration in nitrites. Additionally, Yu et al. [40, 52] assigned a broad band at 1660–1680 cm^{-1} as the C=O vibration in amide overlapping with the N=O vibration in nitrites. Gebald et al. [42, 54] assigned a similar peak (1670 cm^{-1}) as the C=N vibration in oxime/imine/nitrile and the C=O vibration in amide/imide. Calleja et al. [43] assigned a similar peak at 1667 cm^{-1} as the C=N stretching vibration of imine, oxime, and/or nitrone. Assignment of this peak (1666 cm^{-1}) in the DRIFT spectra of BPEI-SiO_2 (10% O_2) is difficult based solely on relevant literature results. Therefore, further analysis was performed.

Figure 2b shows a weak peak at 1560 cm^{-1} for LPEI-SiO_2, attributed to the COO^- stretching vibration in carbamate due to adsorption of CO_2 from the atmosphere [56]. However, the peak becomes more prominent for LPEI-SiO_2(15% CO_2) and LPEI-SiO_2(10% O_2) due to the C-N stretching vibration of urea linkages [53–55, 59]. In the DRIFT spectra of LPEI-SiO_2 and LPEI-SiO_2(15% CO_2),

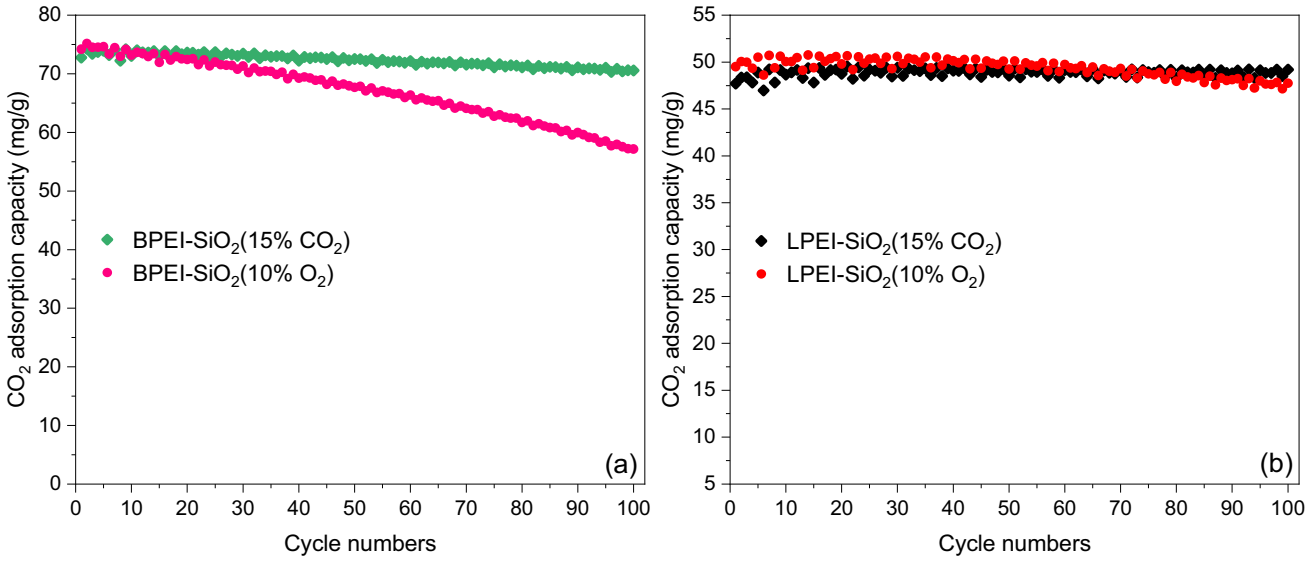

Fig. 1 CO_2 cyclic adsorption–desorption results for **a** BPEI-SiO_2(15% CO_2) and BPEI-SiO_2(10% O_2) and **b** LPEI-SiO_2(15% CO_2) and LPEI-SiO_2(10% O_2)

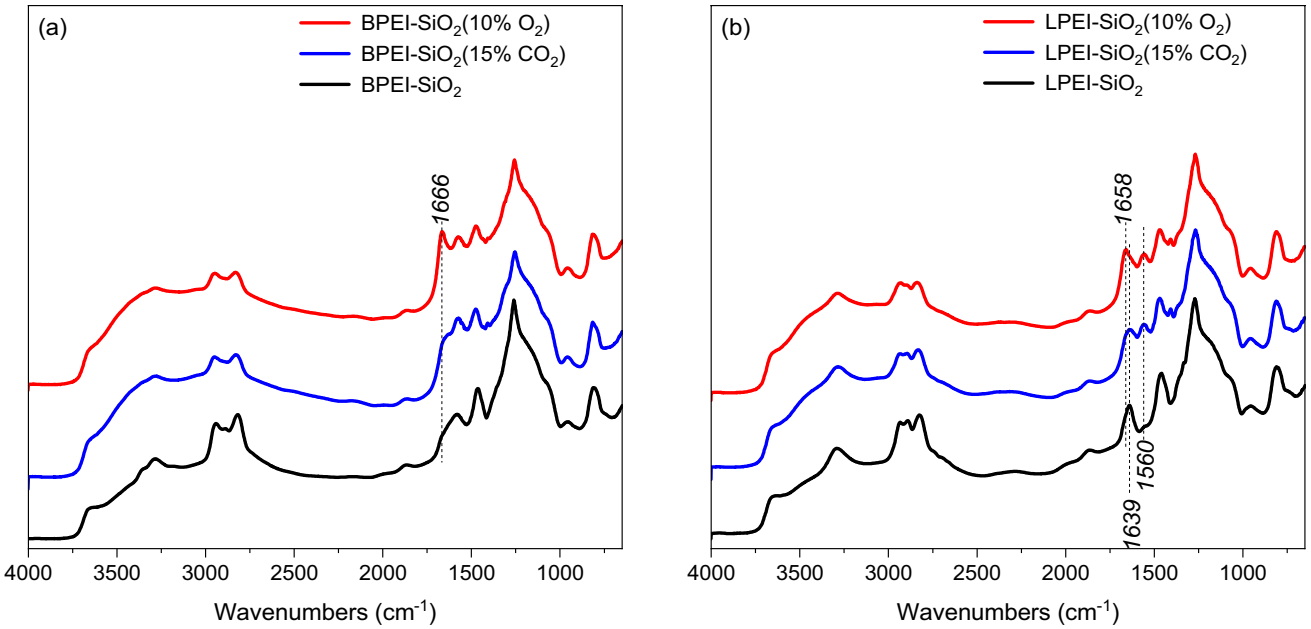

Fig. 2 DRIFT spectra of **a** BPEI-SiO_2, BPEI-SiO_2(15% CO_2), and BPEI-SiO_2(10% O_2) and **b** LPEI-SiO_2, LPEI-SiO_2(15% CO_2), and LPEI-SiO_2(10% O_2)

a peak at 1639 cm^{-1}, attributed to the N–H deformation vibration of the secondary amine in LPEI [60], was observed. However, in the IR spectra of LPEI-SiO_2(10% O_2), the peak at 1639 cm^{-1} is obscured by a prominent peak at 1658 cm^{-1}, most likely the C=O stretching vibration from the oxidization of LPEI-SiO_2.

Figure 3a and b show the in situ DRIFT spectra of BPEI-SiO_2 and LPEI-SiO_2 when interacting with gas 1 (15% CO_2 balanced with N_2). No apparent changes in the DRIFT spectra were observed during the interaction. After regeneration, the flat line spectrum in Fig. 3a indicated no noticeable degradation induced by CO_2. In Fig. 3b, a negative

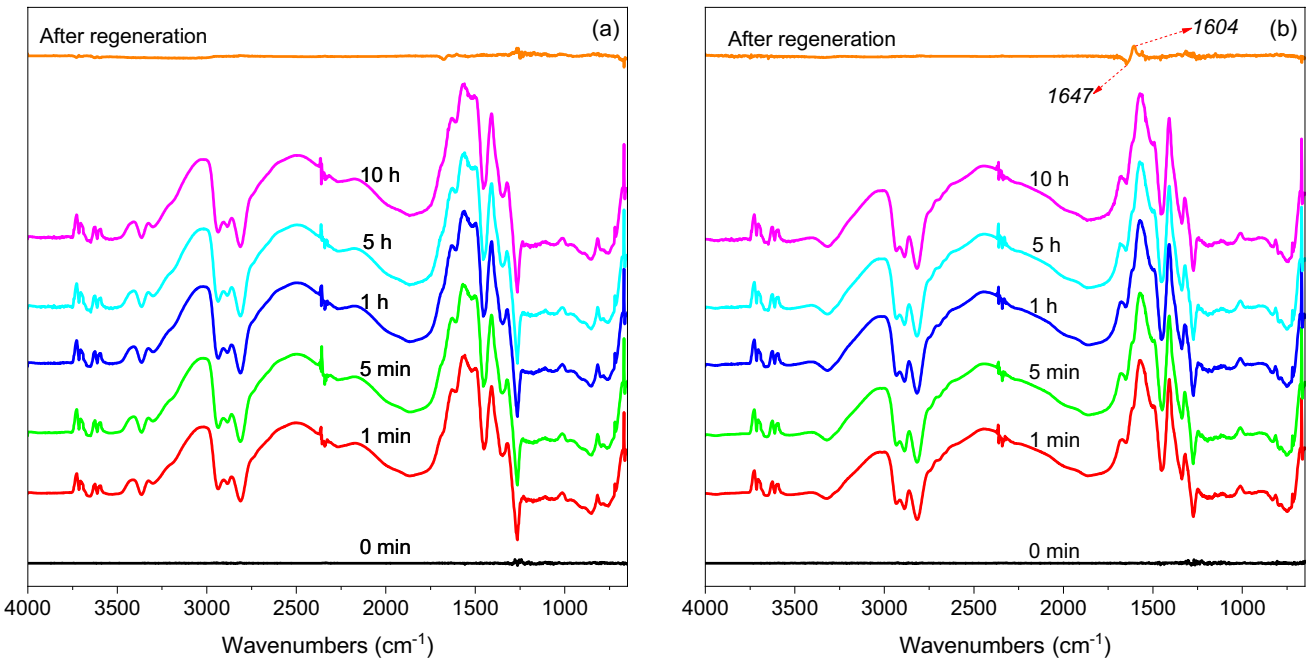

Fig. 3 In situ DRIFT spectra of **a** BPEI-SiO_2 and **b** LPEI-SiO_2 when interacting with gas 1 (15% CO_2 balanced with N_2)

peak at 1647 cm^{-1} and a positive peak at 1604 cm^{-1} were observed after regeneration, which is most likely due to the removal of chemically adsorbed H_2O in LPEI-SiO_2.

Figure 4a and b show the in situ DRIFT spectra of BPEI-SiO_2 and LPEI-SiO_2, respectively, when interacting with 10% O_2 (15% CO_2 and 10% O_2 balanced with N_2). No apparent changes in the DRIFT spectra were observed during the interaction. After a 10-h interaction, no peaks indicating oxidation by O_2 were observed in the DRIFT spectra of regenerated BPEI-SiO_2. A weak peak at 1670 cm^{-1} in the DRIFT spectra of regenerated LPEI-SiO_2 was attributed to the C=O vibration derived from oxidation by O_2. After a 24-h interaction, the peak size at 1670 cm^{-1} increased in the DRIFT spectra of regenerated LPEI-SiO_2. In the DRIFT spectra of regenerated BPEI-SiO_2, two positive peaks appeared at 1670 cm^{-1} and 1606 cm^{-1} and two negative peaks at 2941 cm^{-1} and 2817 cm^{-1}. The two negative peaks (2941 cm^{-1} and 2817 cm^{-1}) corresponded to the C–H asymmetric and symmetric stretching vibration [56, 61, 62], indicating the loss of $–CH_2–$ groups in BPEI. The positive peak at 1670 cm^{-1} is likely due to the C=O stretching vibration, and the positive peak at 1606 cm^{-1} indicates C=N vibration [37]. We concluded that O_2 oxidizes $–CH_2–$ groups in BPEI to form C=O and can also oxidize $–CH_2–NH–$ to form C=N groups. The C=O pathway seems to dominate based on the absorption intensity of the C=O peak (1670 cm^{-1}), which is much stronger than the C=N peak (1606 cm^{-1}). In LPEI, O_2 oxidizes $–CH_2–$ groups to form a small number of C=O groups.

These results demonstrate that the oxidization of BPEI-SiO_2 and LPEI-SiO_2 is a relatively slow process, but BPEI-SiO_2 is more readily oxidized than LPEI-SiO_2. We speculated that the CO_2 adsorption capacity of LPEI-SiO_2 would also gradually decrease if we increased the test duration.

3.2 The adverse effects of SO_2

Figure 5a and b show the CO_2 adsorption capacity of BPEI-SiO_2 and LPEI-SiO_2 after exposure to SO_2. SO_2 led to a severe decrease in CO_2 adsorption capacity. An almost linear decrease in CO_2 adsorption capacity was observed for both BPEI-SiO_2 and LPEI-SiO_2 after exposure to 10 or 50 ppm SO_2 (15% CO_2 and 10 or 50 ppm SO_2 balanced with N_2). The CO_2 adsorption capacity of BPEI-SiO_2 and LPEI-SiO_2 cumulatively decreased by 18.2% and 18.5% at 10 ppm SO_2 and by 61.4% and 60.6% at 50 ppm SO_2. When the level of SO_2 reached 200 ppm, the CO_2 adsorption capacity of BPEI-SiO_2 and LPEI-SiO_2 respectively lost 89.0% and 78.5%. And the decrease in the CO_2 adsorption capacity occurred mainly in the first 50–60 cycles in the 200 ppm SO_2 scenario. For example, the CO_2 adsorption capacity of BPEI-SiO_2 at the 60th cycle and of LPEI-SiO_2 at the 50th cycle decreased by 85.5% and 74.1%, respectively. During subsequent cycles, the decreasing CO_2 adsorption capacity reached a plateau. The stable CO_2 adsorption performance in the plateaus may be due to the residual isolated amino groups, which could adsorb CO_2 and, more importantly, could adsorb SO_2 reversibly [28, 44, 48, 52].

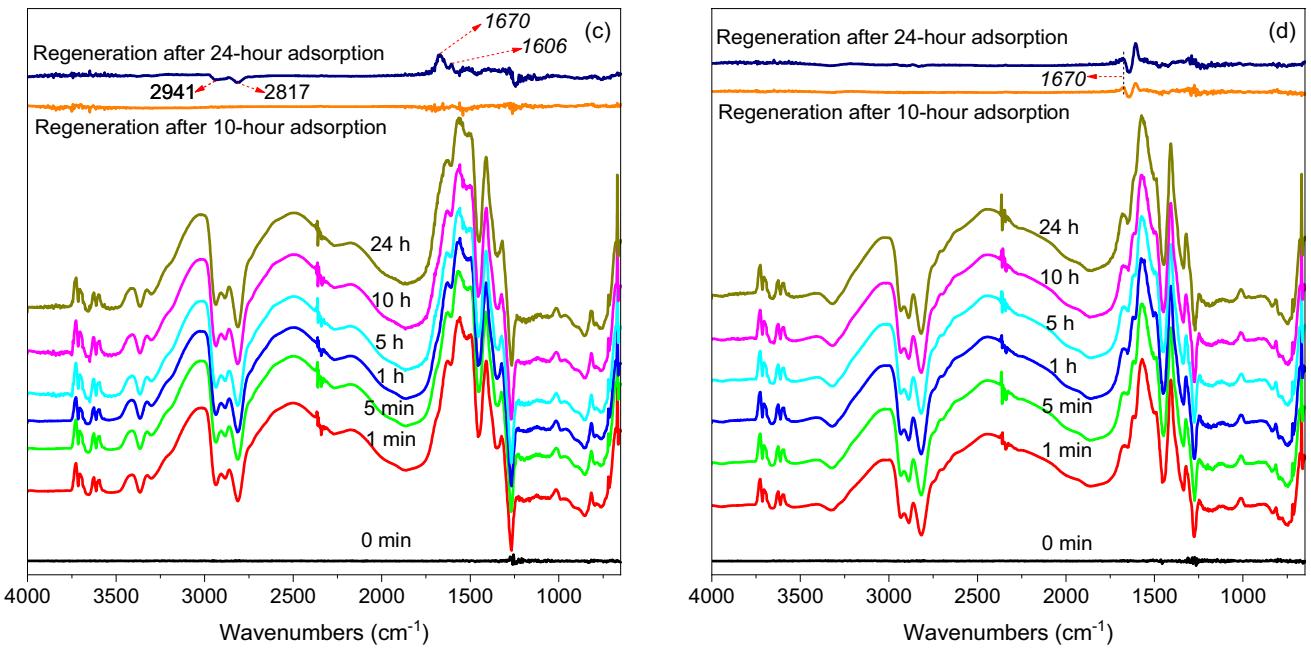

Fig. 4 In situ DRIFT spectra of **a** BPEI-SiO_2, and **b** LPEI-SiO_2 during interaction with 10% O_2 (15% CO_2 and 10% O_2 balanced with N_2)

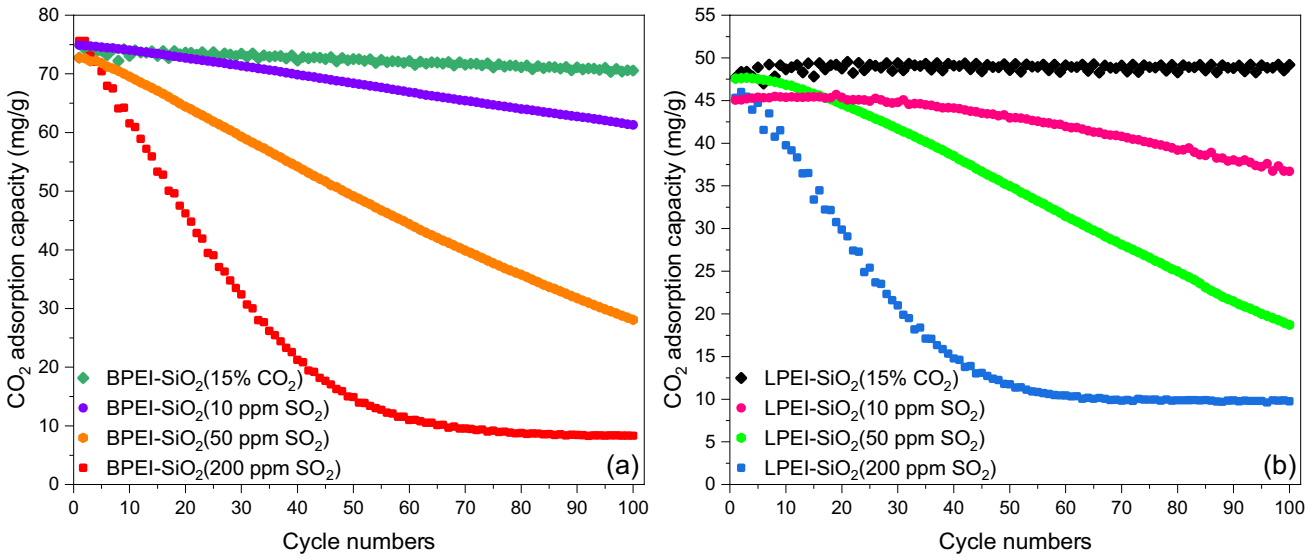

Fig. 5 CO_2 cyclic adsorption–desorption results for **a** BPEI-SiO_2(15% CO_2), BPEI-SiO_2(10 ppm SO_2), BPEI-SiO_2(50 ppm SO_2), and BPEI-SiO_2(200 ppm SO_2) and **b** LPEI-SiO_2(15% CO_2), LPEI-SiO_2(10 ppm SO_2), LPEI-SiO_2(50 ppm SO_2), and LPEI-SiO_2(200 ppm SO_2)

Figure 6a shows a peak at 1662 cm^{-1} for each sample, typically associated with the C=O stretching vibration, but the absorption intensities differed significantly. For BPEI-SiO_2, the peak was derived from the C=O stretching vibration in carbamate and carbamic acid due to adsorption of CO_2 from the atmosphere [13, 52–56]. For BPEI-SiO_2(15% CO_2), the formation of urea linkages was most responsible for the peak [13, 57]. For BPEI-SiO_2(10 ppm SO_2), the peak's adsorption intensity was similar to that for BPEI-SiO_2(15% CO_2). However, for BPEI-SiO_2(50 ppm SO_2) and BPEI-SiO_2(200 ppm SO_2), the peak's intensity increased, likely due to the affinity of SO_2 to BPEI-SiO_2.

A similar phenomenon was observed at 1666 cm^{-1} in Fig. 6b. Meantime, two other peaks at 1496 cm^{-1} and 1560 cm^{-1}, most likely attributed to the C–N stretching vibration of urea linkages [53–55, 59], can also be observed in Fig. 6b. Thus, we postulate that the intense peak at 1666 cm^{-1} for SO_2-exposed samples is due mainly

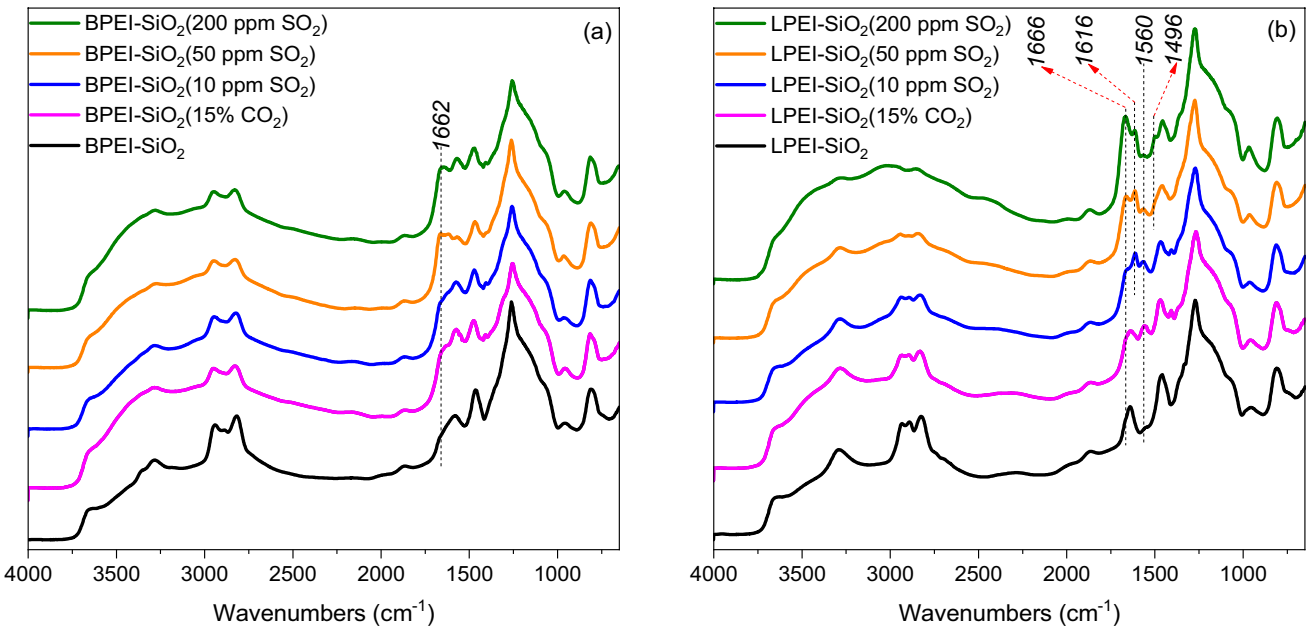

Fig. 6 DRIFT spectra of **a** BPEI-SiO_2, BPEI-SiO_2(15% CO_2), BPEI-SiO_2(10 ppm SO_2), BPEI-SiO_2(50 ppm SO_2), and BPEI-SiO_2(200 ppm SO_2) and **b** LPEI-SiO_2, LPEI-SiO_2(15% CO_2), LPEI-SiO_2(10 ppm SO_2), LPEI-SiO_2(50 ppm SO_2), and LPEI-SiO_2(200 ppm SO_2)

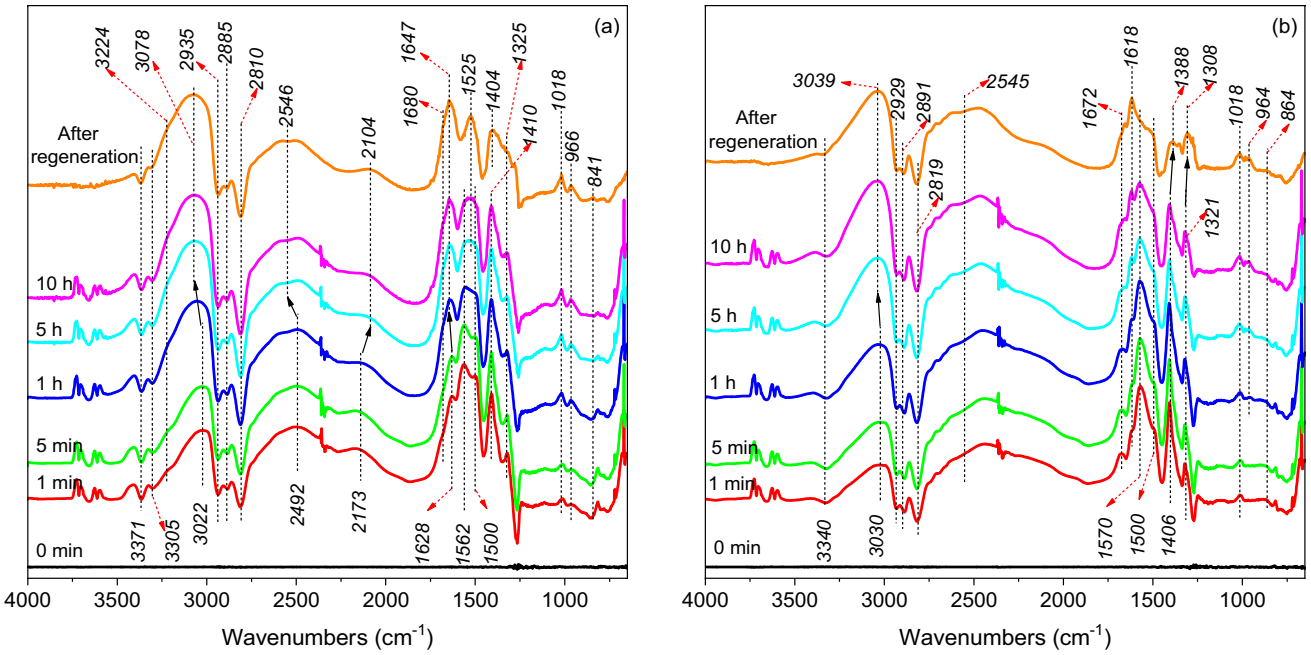

Fig. 7 In situ DRIFT spectra of **a** BPEI-SiO_2 and **b** LPEI-SiO_2 during interaction with 200 ppm SO_2 (15% CO_2 and 200 ppm SO_2 balanced with N_2)

to the C=O stretching vibration of urea linkages. The peak at 1662 cm^{-1} in Fig. 6a may also represent the C=O stretching vibration of urea linkages. Therefore, we concluded that SO_2 promotes the formation of urea linkages when PEI functional adsorbents interact with CO_2 streams containing SO_2. Moreover, NH_2^+ deformation vibrations were observed at 1616 cm^{-1} in the DRIFT spectra of LPEI-SiO_2(10 ppm SO_2), LPEI-SiO_2(50 ppm SO_2), and LPEI-SiO_2 (200 ppm SO_2) [56, 61, 63] in Fig. 6b. These represent the formation of heat-stable NH_2^+-containing adducts between SO_2 and LPEI-SiO_2.

Figure 7a and b show in situ DRIFT spectra of BPEI-SiO_2 and LPEI-SiO_2, respectively, when interacting with 200 ppm SO_2 (15% CO_2 and 200 ppm SO_2 balanced with N_2) at 75 °C. In Fig. 7a, the initial peak at 3022 cm^{-1}, representing the NH_3^+/NH_2^+ vibration [56, 61, 63], clearly strengthened and gradually shifted to 3078 cm^{-1} with prolonged interaction time. Similarly, the initial peak at 1628 cm^{-1}, representing the NH_3^+ vibration [56, 61, 63], clearly strengthened and gradually shifted to 1647 cm^{-1}. After regeneration, the two peaks had a high absorption intensity. The peak at 2546 cm^{-1}, representing the NH_3^+/NH_2^+ vibration [56, 61, 64], and the peak at 2104 cm^{-1}, representing the NH_3^+ vibration [56, 61, 64], were observed after regeneration. The two peaks at 1562 cm^{-1} and 1500 cm^{-1}, which represent the COO^- stretching vibration in carbamate [52, 56, 61, 64–66], disappeared after regeneration, implying the release of the adsorbed CO_2. Therefore, the remaining NH_3^+/NH_2^+ groups must originate from the formation of heat-stable NH_3^+/NH_2^+-containing adducts between BPEI-SiO_2 and SO_2. Meanwhile, the peaks at 1018 cm^{-1} and 966 cm^{-1} most likely belong to the asymmetric and symmetric S=O stretching vibration [22, 45, 46, 63, 67], and the peak at 841 cm^{-1} represents the S–O stretching vibration [46, 68], which all suggest the existence of sulfur-containing products. All of the above peaks are observed at similar locations in Fig. 7b.

The above analysis demonstrates that SO_2 reacted with BPEI and LPEI to form irreversible NH_3^+- and/or NH_2^+-containing adducts. Previous studies reported that sulfites and/or sulfates formed between SO_2 and solid amine adsorbents [17, 44–46, 49, 68]. As H_2O and O_2 were free during the interaction processes in this study, we hypothesized that the following Eqs. (1) and (2) describe a possible mechanism for the reactions between SO_2 and amino groups [44, 69]. These equations are similar to the reaction between CO_2 and amino groups under dry conditions (Eqs. (3) and (4)):

$$R_1R_2NH + SO_2 \leftrightarrow R_1R_2NH^+SOO^- \quad (1)$$

$$R_1R_2NH + R_1R_2NH^+SOO^- \leftrightarrow R_1R_2NH_2^+ + R_1R_2NSOO^- \quad (2)$$

$$R_1R_2NH + CO_2 \leftrightarrow R_1R_2NH^+COO^- \quad (3)$$

$$R_1R_2NH + R_1R_2NH^+COO^- \leftrightarrow R_1R_2NH_2^+ + R_1R_2NCOO^- \quad (4)$$

R_1, R_2 = H or CH_2

The peak at 1680 cm^{-1} in Fig. 7a and at 1672 cm^{-1} in Fig. 7b were both observed after regeneration. They most likely belong to the C=O stretching vibration of urea linkages. In previous research [13], we found that the in situ DRIFT peak representing C=O in urea linkages was extremely weak after 11 h of interaction between pure CO_2 and the BPEI (MW = 600 Da) functional adsorbent at 75 °C. Thus, the intense peaks observed after regeneration must be derived from the influence of SO_2 (Fig. 7a and b). As we had speculated, SO_2 can promote the formation of urea linkages between PEI functional adsorbents and CO_2.

The in situ DRIFT spectra of BPEI-SiO_2 or LPEI-SiO_2 in the presence of 10 ppm SO_2 (15% CO_2 and 10 ppm SO_2 balanced with N_2) are shown in Figures S7, S8, and S9 in the Supplementary Information. The spectra were similar to those in the 200 ppm SO_2 scenario, but the absorption intensity was much lower in the 10 ppm SO_2 scenario.

3.3 The adverse effects of NO_2

Generally, NO_2 accounts for only 5% or less of the total NO_x in flue gas [70]. In this study, we used a concentration of 10 ppm NO_2 (15% CO_2 and 10 ppm NO_2 balanced with N_2) to investigate the adverse effects of NO_2 on PEI functional adsorbents. As a reference, 200 ppm NO_2 (15% CO_2 and 200 ppm NO_2 balanced with N_2) was also investigated. CO_2 cyclic adsorption–desorption tests (Fig. 8a and b) showed excellent CO_2 adsorption stabilities for both BPEI-SiO_2 and LPEI-SiO_2 under the 10 ppm NO_2 scenario. However, under the 200 ppm NO_2 scenario, the CO_2 adsorption capacity of BPEI-SiO_2 and LPEI-SiO_2 showed an almost linear decline and were decreased by 49.6% and 49.5%, respectively.

In Fig. 9a and b, a sharp peak at 1666 cm^{-1} was observed for both BPEI-SiO_2(200 ppm NO_2) and LPEI-SiO_2(200 ppm NO_2). The peaks are possibly associated with the C=O stretching vibration in urea linkages. However, in the presence of NO_2, it is difficult to exclude the N=O stretching vibration in nitrites and/or nitrates for this peak (1666 cm^{-1}) [63]. Furthermore, a peak at approximately 1361 cm^{-1} was observed in the DRIFT spectra of BPEI-SiO_2(200 ppm NO_2) and LPEI-SiO_2(200 ppm NO_2), most likely associated with the formation of N-nitroso compounds [71, 72]. In Fig. 9a, the DRIFT spectra of BPEI-SiO_2(10 ppm NO_2) are similar to those of BPEI-SiO_2 (15% CO_2). In Fig. 9b, a peak at 1612 cm^{-1}, representing the NH_2^+ deformation vibration [56, 61, 63], was observed for both LPEI-SiO_2(10 ppm NO_2) and LPEI-SiO_2(200 ppm NO_2), but not for LPEI-SiO_2 or LPEI-SiO_2(15% CO_2).

Figure 10a and b exhibit the in situ DRIFT spectra of BPEI-SiO_2 and LPEI-SiO_2 during interaction with 200 ppm NO_2 (15% CO_2 and 200 ppm NO_2 balanced with N_2). Figure 10a shows that the initial peak at 3022 cm^{-1} gradually strengthened and shifted to 3074 cm^{-1} during prolonged interaction time. This peak represents the NH_3^+/NH_2^+ stretching vibration [56, 61, 63] and was still prominent after regeneration. The peak at approximately 2505 cm^{-1} represents the NH_3^+/NH_2^+ stretching vibration [56, 61, 64], and the peaks at approximately 2162 cm^{-1} and 1631 cm^{-1} represent the NH_3^+ vibration [56, 61, 63, 64] and were observed after regeneration. The peak at 1651 cm^{-1}, most likely due to the N=O vibration in nitrites and/or nitrates [63], emerged and gradually strengthened with prolonged interaction time, and the sharp peak was still present after regeneration. Furthermore, the peak at

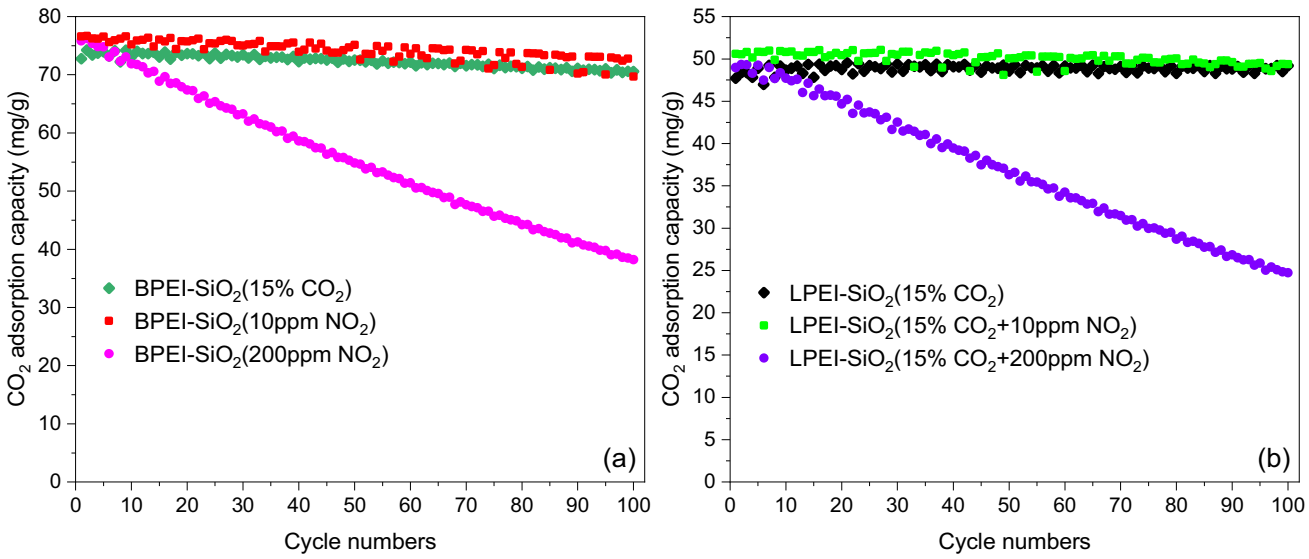

Fig. 8 CO_2 cyclic adsorption–desorption results for **a** BPEI-SiO_2(15% CO_2), BPEI-SiO_2(10 ppm NO_2), and BPEI-SiO_2(200 ppm NO_2) and **b** LPEI-SiO_2(15% CO_2), LPEI-SiO_2(10 ppm NO_2), and LPEI-SiO_2(200 ppm NO_2)

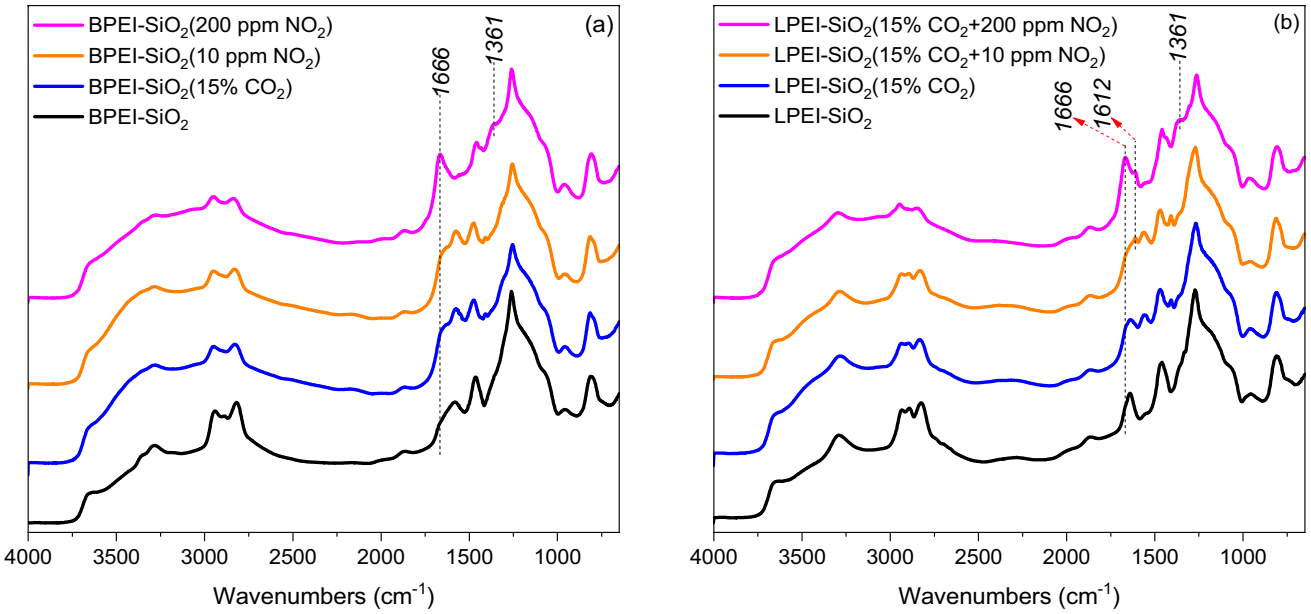

Fig. 9 DRIFT spectra of **a** BPEI-SiO_2, BPEI-SiO_2(15% CO_2), BPEI-SiO_2(10 ppm NO_2), and BPEI-SiO_2(200 ppm NO_2) and **b** LPEI-SiO_2, LPEI-SiO_2(15% CO_2), LPEI-SiO_2(10 ppm NO_2), and LPEI-SiO_2(200 ppm NO_2)

802 cm^{-1}, representing the C-N stretching vibration in nitrites [63], and the peak at 1126 cm^{-1}, representing N–N stretching vibration in nitrates [46, 63], both remained after regeneration.

All of the above peaks are observed at similar locations in Fig. 10b. Therefore, the formation of NH_3^+ and/or NH_2^+-containing nitrites and/or nitrates is an important route for the degradation of BPEI-SiO_2 and LPEI-SiO_2. Considering O_2 and H_2O are free during the interaction processes, we speculate that the possible formation mechanism of nitrites and nitrates is depicted in Eqs. (5) to (9) [73]:

$$R_1R_2NH + NO_2 \leftrightarrow R_1R_2NH^+NOO^- \quad (5)$$

$$R_1R_2NH + R_1R_2NH^+NOO^- \leftrightarrow R_1R_2NH_2^+ + R_1R_2NNOO^- \quad (6)$$

$$NO_2^{\cdot} + NO_2^{\cdot} \leftrightarrow N_2O_4 \quad (7)$$

$$R_1R_2NH + N_2O_4 \leftrightarrow R_1R_2NH^+NOOO^- + NO \quad (8)$$

$$R_1R_2NH + R_1R_2NH^+NOOO^- \leftrightarrow R_1R_2NH_2^+ + R_1R_2NNOOO^- \quad (9)$$

R_1, R_2 = H or CH_2

In Fig. 10a, the peaks at 1525 cm^{-1}, 1396 cm^{-1}, and 1246 cm^{-1} may represent different types of NO_2 stretching vibrations in N-nitro compounds (N-NO_2) [22, 63]. Corresponding peaks are observed at 1525 cm^{-1}, 1400 cm^{-1}, and 1242 cm^{-1} in Fig. 10b. Meanwhile, the peak at 962 cm^{-1} in Fig. 10a and the peak at 957 cm^{-1} in Fig. 10b may represent the N–N stretching vibration in N-nitro compounds [63]. Moreover, in Fig. 10a, the two peaks at 1525 cm^{-1} and 1396 cm^{-1} may also represent NO_2 asymmetric and symmetric stretching vibrations in C-nitro compounds (C–NO_2) [63]. The peak at 1377 cm^{-1} may represent the N=O stretching vibration in C-nitroso compounds (C-NO) [63], with the C-nitro and C-nitroso compounds arising due to the oxidation of NO_2 to a primary amine in BPEI. N_2O_4 may also act as an oxidizing agent.

The peaks at 1680 cm^{-1} in Fig. 10a and 1676 cm^{-1} in Fig. 10b were observed after regeneration. The two peaks are most likely due to the C=O stretching vibration in urea linkages. These two peaks were mutually corroborative with the two peaks at 1666 cm^{-1} in Fig. 9a and b. Therefore, similar to SO_2, NO_2 also promotes the formation of urea linkages between PEI functional adsorbents and CO_2.

At 3215 cm^{-1} in Fig. 10a and 3190 cm^{-1} in Fig. 10b, apparent variations are observed. These two peaks gradually strengthened and can be observed after regeneration. A similar observation was noted at 3224 cm^{-1} in Fig. 7a. These peaks most likely represent the O–H vibration in acid. We hypothesized that the following Eqs. (10) to (15) might explain the appearance of the peak:

$$RNH_2 + CO_2 \leftrightarrow RNH_2^+COO^- \leftrightarrow RHNCOOH \quad (10)$$

$$RNH_2 + SO_2 \leftrightarrow RNH_2^+SOO^- \leftrightarrow RHNSOOH \quad (11)$$

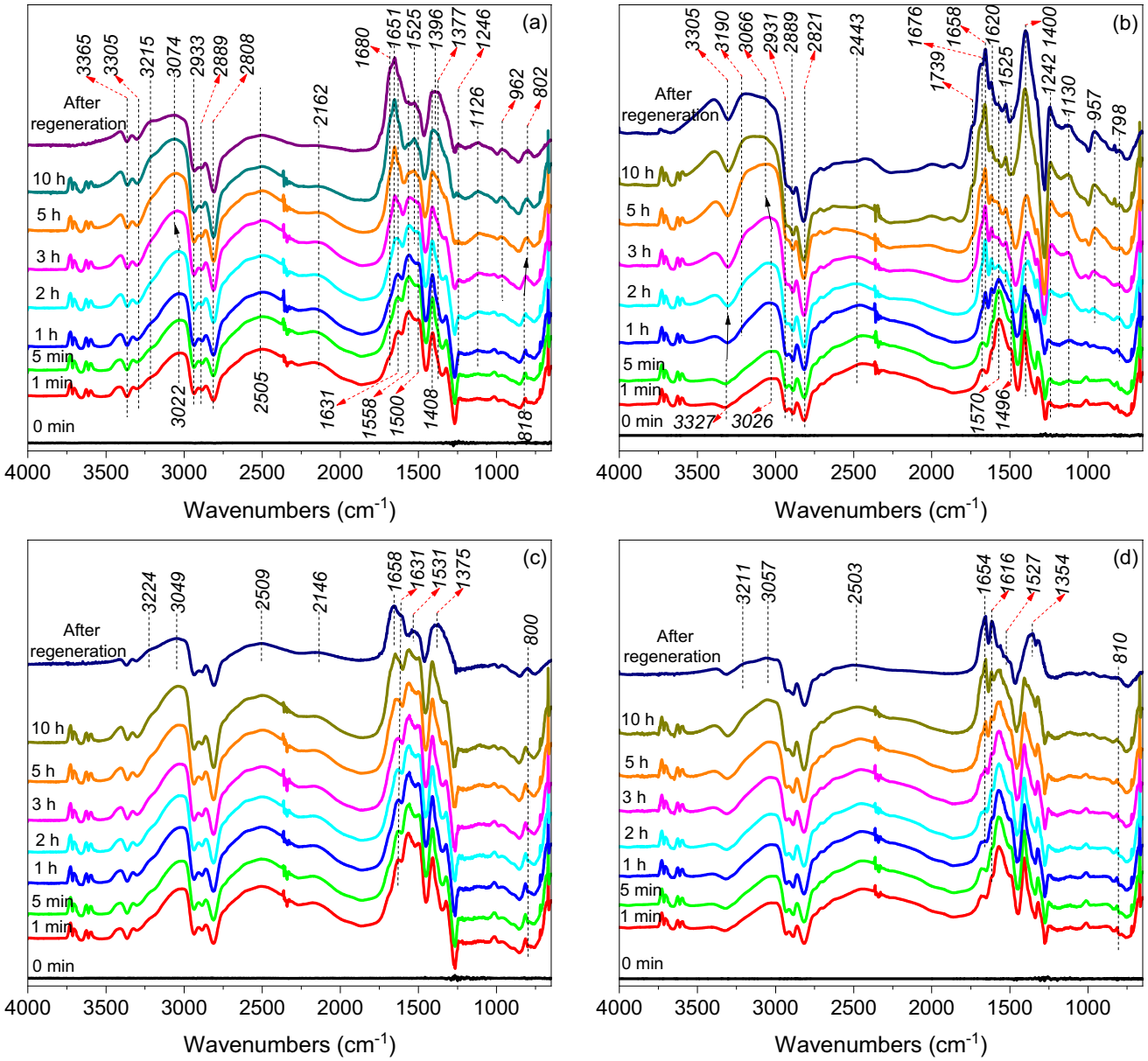

Fig. 10 In situ DRIFT spectra of **a** BPEI-SiO_2 and **b** LPEI-SiO_2 when interacting with 200 ppm NO_2 (15% CO_2 and 200 ppm NO_2 balanced with N_2) and of **c** BPEI-SiO_2 and (d) LPEI-SiO_2 when interacting with 10 ppm NO_2 (15% CO_2 and 10 ppm NO_2 balanced with N_2)

$$R_1R_2NH + NO_2 \leftrightarrow R_1R_2NH^+NOO^- \leftrightarrow R_1R_2NNOOH \quad (12)$$

$$NO_2^{\cdot} + NO_2^{\cdot} \leftrightarrow N_2O_4 \quad (13)$$

$$R_1R_2NH_2 + N_2O_4 \leftrightarrow R_1R_2NH^+NOOO^- + NO \quad (14)$$

$$R_1R_2NH^+NOOO^- \leftrightarrow R_1R_2NNOOOH \quad (15)$$

$R_1, R_2 = H$ or CH_2

Figure 10 c and d show in situ DRIFT spectra during interaction with 10 ppm NO_2 (15% CO_2 and 10 ppm NO_2 balanced with N_2) for BPEI-SiO_2 and LPEI-SiO_2. The spectra are similar to those in Fig. 10a and b, but with a much weaker absorption intensity. Therefore, 10 ppm NO_2 could also lead to degradation of BPEI-SiO_2 and LPEI-SiO_2 via similar mechanisms. The degradation induced by 10 ppm NO_2 was very slight, and therefore no pronounced decrease in the CO_2 adsorption capacity was observed. However, when the CO_2 cyclic adsorption–desorption cycles were increased, both BPEI-SiO_2 and LPEI-SiO_2 encountered a

loss in their CO_2 adsorption capacity under the 10 ppm NO_2 scenario

3.4 The adverse effects of NO

As mentioned above, NO typically accounts for over 95% of the total NO_x in flue gas. We only investigated the impact of 200 ppm NO on BPEI-SiO_2 and LPEI-SiO_2. Figure 11a and b show the changes in the CO_2 adsorption capacity of BPEI-SiO_2 and LPEI-SiO_2 after exposure to 200 ppm NO (15% CO_2 and 200 ppm NO balanced with N_2). The CO_2 adsorption performance of BPEI-SiO_2 and LPEI-SiO_2 was very stable during the whole process.

In Fig. 12a and b, the DRIFT spectrum of BPEI-SiO_2(200 ppm NO) is similar to that of BPEI-SiO_2(15% CO_2), while the DRIFT spectrum of LPEI-SiO_2(200 ppm NO) is similar to that of LPEI-SiO_2(15% CO_2). Compared with the DRIFT spectra of BPEI-SiO_2, the absorption intensity of the peak at approximately 1666 cm^{-1} was stronger in the DRIFT spectra of BPEI-SiO_2(200 ppm NO) and BPEI-SiO_2 (15% CO_2). The sharp peak at 1558 cm^{-1} was far more prominent for LPEI-SiO_2(200 ppm NO) and LPEI-SiO_2(15% CO_2) than for LPEI-SiO_2. These two peaks at 1666 cm^{-1} and 1558 cm^{-1} represent the C=O stretching vibration and the C-N stretching vibration in urea linkages. This is due mainly to the formation of urea linkages during the CO_2 cyclic adsorption–desorption processes. The DRIFT spectra provide no information on the degradation induced by NO.

Figure 13a and b show the in situ DRIFT spectra for BPEI-SiO_2 and LPEI-SiO_2 during interaction with 200 ppm NO (15% CO_2 and 200 ppm NO balanced with N_2). No apparent changes were observed for BPEI-SiO_2 or LPEI-SiO_2 during the interaction processes. But some peaks remained after regeneration in Fig. 13a, for example, the peaks at 2985 cm^{-1} and 2509 cm^{-1} denoting the NH_3^+/NH_2^+ vibration [56, 61, 64], the peak at 1657 cm^{-1} representing the N=O vibration [63], the peak at 1606 cm^{-1} most likely denoting the NH_2^+ vibration, and the peak at 1011 cm^{-1} likely representing the N–N stretching vibration. All of these peaks were observed at similar locations in Fig. 13b. Equations (16) to (18), shown below, may provide an explanation for these peaks [69]. The reaction in Eq. (16) limited the formation of $R_1R_2NH_2^+$ $R_1R_2NHN_2O_2^-$ and further confined the degradation of BPEI-SiO_2 and LPEI-SiO_2 induced by NO.

$$R_1R_2NH + NO \leftrightarrow R_1R_2NHNO\,(\text{slow}) \tag{16}$$

$$R_1R_2NHNO + NO \leftrightarrow R_1R_2NHN_2O_2(\text{fast}) \tag{17}$$

$$R_1R_2NHN_2O_2 + R_1R_2NH \leftrightarrow R_1R_2NH_2^+R_1R_2NHN_2O_2^-(\text{fast}) \tag{18}$$

R_1, R_2 = H or CH_2

Furthermore, the peak at 1361 cm^{-1} in Fig. 13a and the peak at 1360 cm^{-1} in Fig. 13b may be associated with the formation of N-nitroso compounds (N–N=O) [71, 72]. These results demonstrate that NO can lead to degradation of PEI functional adsorbents by forming $R_1R_2NH_2^+$ $R_1R_2NHN_2O_2^-$ and N-nitroso compounds. However, the degradation induced by NO was extremely low and

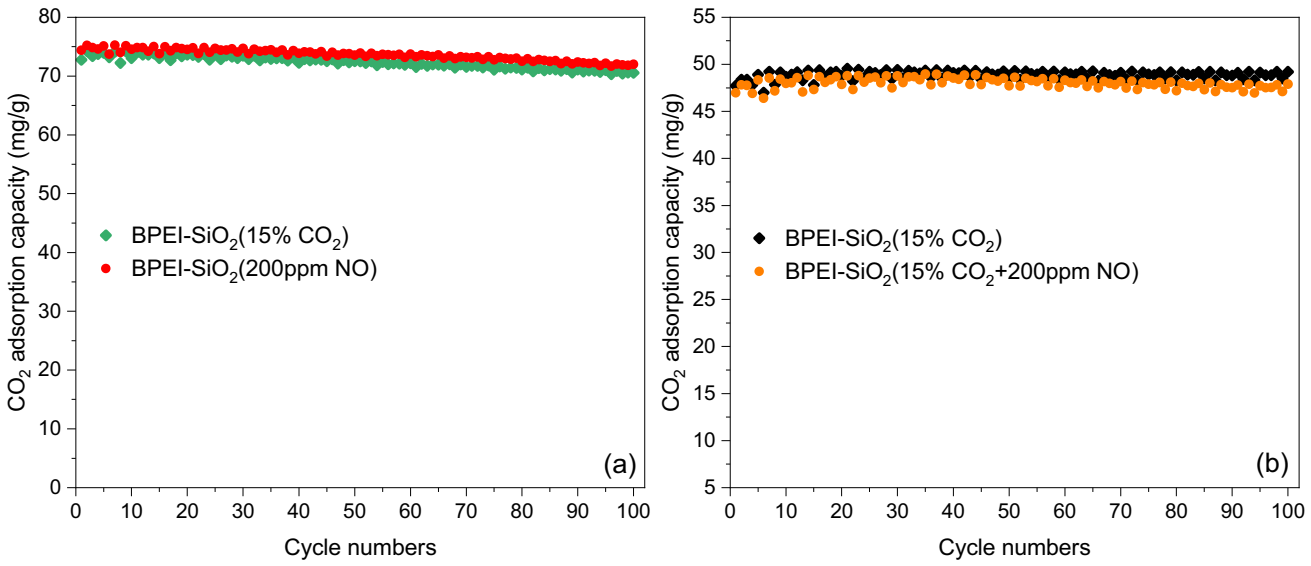

Fig. 11 CO_2 cyclic adsorption–desorption results for **a** BPEI-SiO_2(15% CO_2) and BPEI-SiO_2(200 ppm NO) and **b** LPEI-SiO_2(15% CO_2) and LPEI-SiO_2(200 ppm NO)

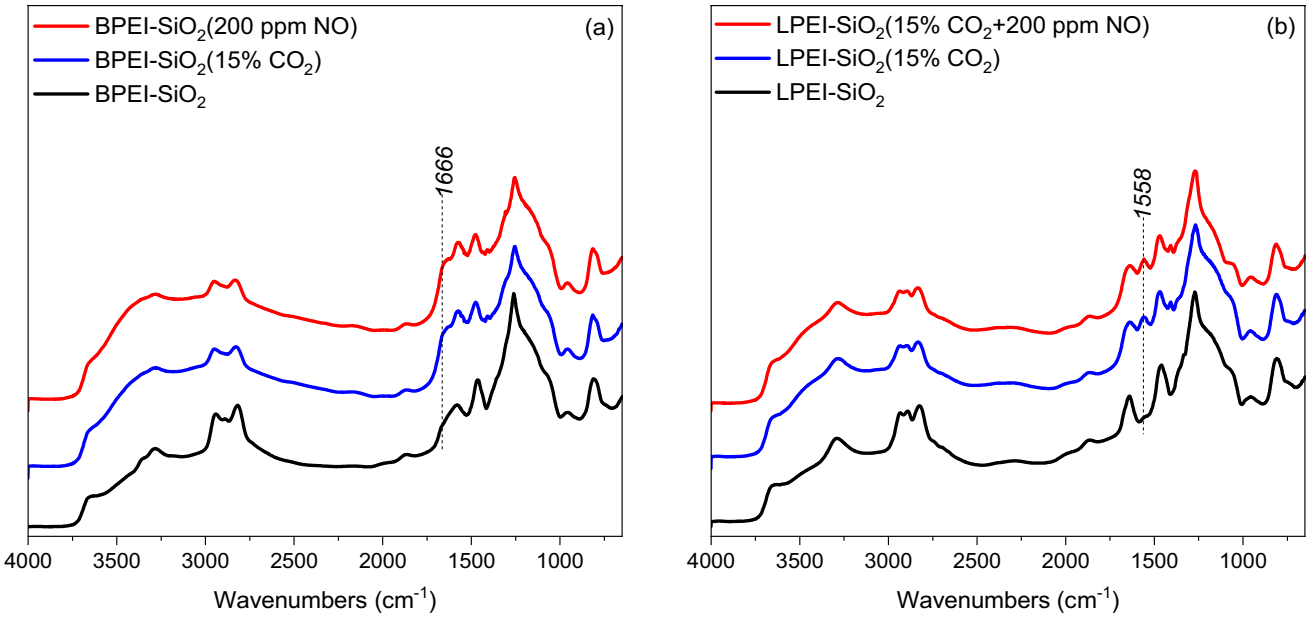

Fig. 12 DRIFT spectra of **a** BPEI-SiO_2, BPEI-SiO_2(15% CO_2), and BPEI-SiO_2(200 ppm NO) and **b** LPEI-SiO_2, LPEI-SiO_2(15% CO_2), and LPEI-SiO_2(200 ppm NO)

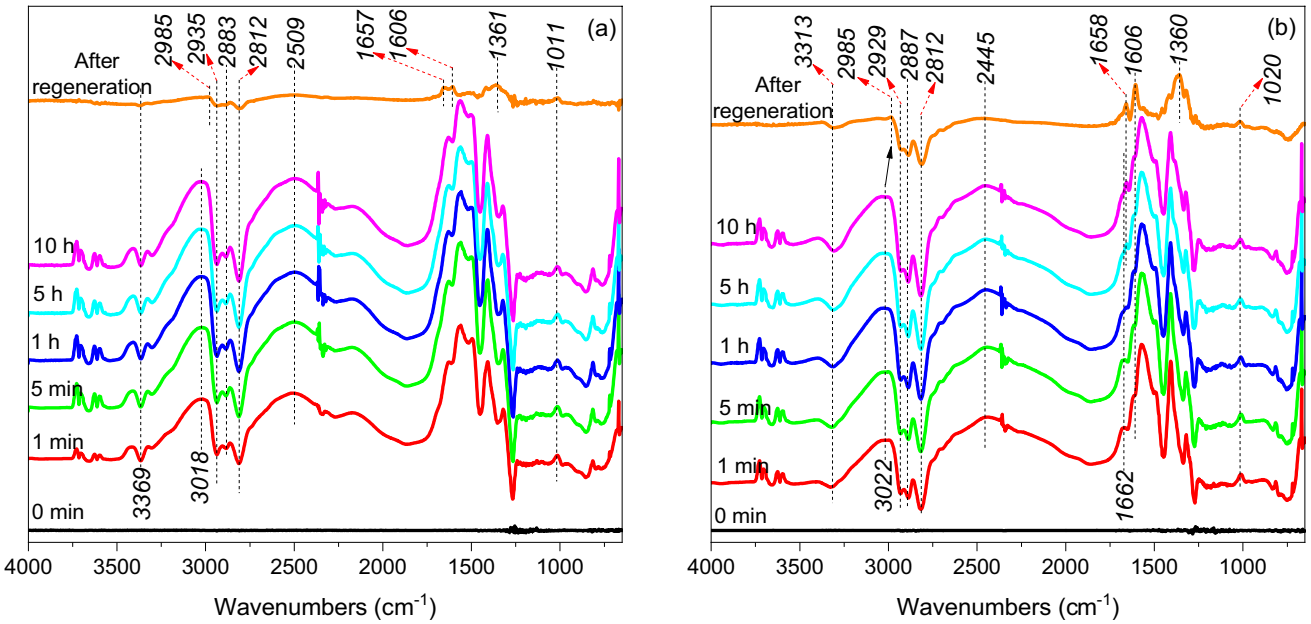

Fig. 13 In situ DRIFT spectra of **a** BPEI-SiO_2, and **b** LPEI-SiO_2 during interaction with 200 ppm NO (15% CO_2 and 200 ppm NO balanced with N_2)

would not cause an obvious decrease in the CO_2 adsorption capacity during the limited duration of CO_2 cyclic adsorption–desorption tests.

4 Conclusions

In this study, the adverse effects of simulated flue gas on BPEI and LPEI functional adsorbents were investigated.

The results showed that O_2, SO_2, NO_2, and NO all caused degradation of PEI functional adsorbents. After contact with 10% O_2 (15% CO_2 and 10% O_2 in N_2) for 990 cumulative minutes, BPEI-SiO_2 lost 23.0% of its original CO_2 adsorption capacity. On the other hand, LPEI-SiO_2 maintained a stable CO_2 adsorption performance during the adsorption process and only lost approximately 3.6% of its original adsorption capacity. However, the IR spectra demonstrated that 10% O_2 also damages LPEI-SiO_2. Three concentration gradients were considered for SO_2, namely 10, 50, and 200 ppm SO_2 (15% CO_2 and 10, 50, or 200 ppm SO_2 in N_2). Higher concentrations of SO_2 would lead to more severe and quicker degradation of BPEI-SiO_2 and LPEI-SiO_2. After contact with 10, 50, or 200 ppm SO_2 for 990 cumulative minutes, BPEI-SiO_2 lost 18.2%, 61.4%, and 89.0% of its original CO_2 adsorption capacity, and LPEI-SiO_2 lost 18.5%, 60.6%, and 78.5% of its original CO_2 adsorption capacity, respectively. As for NO_x, 10 ppm NO_2 (15% CO_2 and 10 ppm NO_2 in N_2) and 200 ppm NO (15% CO_2 and 200 ppm NO in N_2) caused almost no decrease in the CO_2 adsorption capacity after 990-min interactions, but as shown by the IR spectra, both concentrations induced degradation of BPEI-SiO_2 and LPEI-SiO_2. We also investigated 200 ppm NO_2 (15% CO_2 and 200 ppm NO_2 in N_2) and observed a 49.6% and 49.5% decrease in the original CO_2 adsorption capacity of BPEI-SiO_2 and LPEI-SiO_2, respectively.

Further exploration of the degradation mechanism demonstrated that O_2 oxidized the $-CH_2-$ and $-CH_2-NH-$ groups of BPEI-SiO_2 to form C=O and C=N groups, and C=O formation seems to be the primary pathway. For LPEI-SiO_2, only C=O formation via oxidation of $-CH_2-$ was observed. SO_2 can react with the amine groups of BPEI-SiO_2 and LPEI-SiO_2 to form heat-stable NH_3^+—and/or NH_2^+—containing adducts. SO_2 can promote the formation of urea linkages between PEI functional adsorbents and CO_2. Similar to SO_2, the presence of NO_2 can lead to the formation of heat-stable NH_3^+—and/or NH_2^+—containing adducts and promote urea linkage formation. Furthermore, NO_2 can result in the formation of heat-stable acid adducts and, likely, N-nitro (N–NO_2), C-nitroso (C–N=O), and C-nitro (C–NO_2) compounds. NO can lead to the formation of heat-stable NH_3^+—and/or NH_2^+—containing adducts, as well as N-nitroso (N–N=O) compounds.

5 Supplementary Information

Molecular structures of BPEI and LPEI are shown in Scheme S1. Detailed in situ DRIFT spectra of BPEI-SiO_2 and LPEI-SiO_2 during interaction with different gas mixtures are shown in Figure S1 to S15.

Acknowledgements The authors are really grateful for the supports of the Postdoctoral Fellowship Scheme of The Hong Kong Polytechnic University (Scheme No. G-YW3U). And the authors sincerely acknowledge the supports from Shanghai Tongji Gao Tingyao Environmental Science & Technology Development Foundation.

Compliance with ethical standards

Conflict of interest The authors declare that there is no any competing interest.The English in this document has been checked by at least two professional editors, both native speakers of English. For a certificate, please see: http://www.textcheck.com/certificate/HjvYgi

References

1. International Engergy Agency, Energy Technology Perspectives (2020 https://www.iea.org/reports/energy-technology-perspectives-2020. September 2020.
2. Murge P, Dinda S, Roy S (2019) Zeolite-based sorbent for co$_2$ capture: preparation and performance evaluation. Langmuir 35(46):14751–14760
3. Megias-Sayago C, Bingre R, Huang L, Lutzweiler G, Wang Q, Louis B (2019) CO_2 Adsorption capacities in zeolites and layered double hydroxide materials. Fron Chem 7:551
4. You YY, Liu XJ (2019) Modeling of CO_2 adsorption and recovery from wet flue gas by using activated carbon. Chem Eng J 369:672–685
5. Gunawan T, Wijiyanti R, Widiastuti N (2018) Adsorption-desorption of CO_2 on zeolite-Y-templated carbon at various temperatures. RSC Adv 8(72):41594–41602
6. Tan P, Jiang Y, Liu X, Sun LB (2019) Making porous materials respond to visible light. ACS Energy Lett 4(11):2656–2667
7. Hu Z, Wang Y, Shah BB, Zhao D (2019) CO2 capture in metal–organic framework adsorbents: an engineering perspective. Adv Sustain Syst 3(1):1800080
8. Perejon A, Romeo LM, Lara Y, Lisbona P, Martinez A, Valverde JM (2016) The Calcium-Looping technology for CO_2 capture: On the important roles of energy integration and sorbent behavior. Appl Energy 162:787–807
9. Arias B, Alonso M, Abanades C (2017) CO_2 Capture by calcium looping at relevant conditions for cement plants: experimental testing in a 30 kW(th) pilot plant. Ind Eng Chem Res 56(10):2634–2640
10. Jiang Y, Tan P, Qi SC, Liu XQ, Yan JH, Fan F, Sun LB (2019) Metal-organic frameworks with target-specific active sites switched by photoresponsive motifs: efficient adsorbents for tailorable CO_2 capture. Angew Chem-Int Edn 58(20):6600–6604
11. Jiang Y, Shi XC, Tan P, Qi SC, Gu C, Yang T, Peng SS, Liu XQ, Sun LB (2020) Controllable CO_2 capture in metal-organic frameworks:

making targeted active sites respond to light. Ind Eng Chem Res 59(50):21894–21900
12. Bos MJ, Kroeze V, Sutanto S, Brilman DWF (2018) Evaluating regeneration options of solid amine sorbent for CO_2 removal. Ind Eng Chem Res 57(32):11141–11153
13. Li KM, Jiang JG, Chen XJ, Gao YC, Yan F, Tian SC (2016) Research on urea linkages formation of amine functional adsorbents during CO_2 capture process: two key factors analysis, temperature and moisture. J Phys Chem C 120(45):25892–25902
14. Goeppert A, Meth S, Prakash GKS, Olah GA (2010) Nanostructured silica as a support for regenerable high-capacity organoamine-based CO_2 sorbents. Energ Environ Sci 3(12):1949–1960
15. Didas SA, Zhu RS, Brunelli NA, Sholl DS, Jones CW (2014) Thermal, oxidative and CO_2 induced degradation of primary amines used for CO_2 capture: effect of alkyl linker on stability. J Phys Chem C 118(23):12302–12311
16. Sjostrom S, Krutka H (2010) Evaluation of solid sorbents as a retrofit technology for CO_2 capture. Fuel 89(6):1298–1306
17. Khatri RA, Chuang SSC, Soong Y, Gray M (2006) Thermal and chemical stability of regenerable solid amine sorbent for CO_2 capture. Energy Fuels 20(4):1514–1520
18. Anderson JL, Dixon JK, Maginn EJ, Brennecke JF (2006) Measurement of SO_2 solubility in ionic liquids. J Phys Chem B 110(31):15059–15062
19. Stevens L, Williams K, Han WY, Drage T, Snape C, Wood J, Wang JW (2013) Preparation and CO_2 adsorption of diamine modified montmorillonite via exfoliation grafting route. Chem Eng J 215:699–708
20. Uyanga IJ, Idem RO (2007) Studies of SO_2- and O_2-induced degradation of aqueous MEA during CO_2 capture from power plant flue gas streams. Ind Eng Chem Res 46(8):2558–2566
21. Bollini P, Choi S, Drese JH, Jones CW (2011) Oxidative degradation of aminosilica adsorbents relevant to postcombustion CO_2 capture. Energy Fuels 25(5):2416–2425
22. Miller DD, Chuang SSC (2015) Experimental and theoretical investigation of SO_2 adsorption over the 1,3-phenylenediamine/SiO_2 system. J Phys Chem C 119(12):6713–6727
23. Rao AB, Rubin ES (2002) A technical, economic, and environmental assessment of amine-based CO_2 capture technology for power plant greenhouse gas control. Environ Sci Technol 36(20):4467–4475
24. Lin KYA, Petit C, Park AHA (2013) Effect of SO_2 on CO_2 capture using liquid-like nanoparticle organic hybrid materials. Energy Fuels 27(8):4167–4174
25. Su FS, Lu CS, Chen HS (2011) Adsorption, desorption, and thermodynamic studies of CO_2 with high-amine-loaded multiwalled carbon nanotubes. Langmuir 27(13):8090–8098
26. Schreiber A, Zapp P, Kuckshinrichs W (2009) Environmental assessment of German electricity generation from coal-fired power plants with amine-based carbon capture. Int J Life Cycle Assess 14(6):547–559
27. Liu YM, Ye Q, Shen M, Shi JJ, Chen J, Pan H, Shi Y (2011) Carbon Dioxide capture by functionalized solid amine sorbents with simulated flue gas conditions. Environ Sci Technol 45(13):5710–5716
28. Fan YF, Labreche Y, Lively RP, Jones CW, Koros WJ (2014) Dynamic CO_2 adsorption performance of internally cooled silica-supported poly(ethylenimine) hollow fiber sorbents. Aiche J 60(11):3878–3887
29. Hallenbeck AP, Kitchin JR (2013) Effects of O_2 and SO_2 on the capture capacity of a primary-amine based polymeric co_2 sorbent. Ind Eng Chem Res 52(31):10788–10794
30. Chandan PA, Remias JE, Liu KL (2014) Possible ways to minimize nitrosation reactions during post-combustion CO_2 capture process. Int J Greenh Gas Con 31:61–66
31. Liu YM, Lin XY, Wu XH, Liu MY, Shi RH, Yu XJ (2017) Pentaethylenehexamine loaded SBA-16 for CO_2 capture from simulated flue gas. Powder Technol 318:186–192
32. Yang J, Yu XH, Yan JY, Tu ST, Dahlquist E (2013) Effects of SO_2 on CO_2 capture using a hollow fiber membrane contactor. Appl Energy 112:755–764
33. Wang ZM, Mitch WA (2015) Influence of dissolved metals on n-nitrosamine formation under amine-based CO_2 capture conditions. Environ Sci Technol 49(19):11974–11981
34. Gouedard C, Picq D, Launay F, Carrette PL (2012) Amine degradation in CO_2 capture I. a review. Int J Greenh Gas Con 10:244–270
35. Chi S, Rochelle GT (2002) Oxidative degradation of monoethanolamine. Ind Eng Chem Res 41(17):4178–4186
36. Dickinson J, Percy A, Puxty G, Verheyen TV (2016) Oxidative degradation of amine absorbents in carbon capture systems—a dynamic modelling approach. Int J Greenh Gas Con 53:391–400
37. Ahmadalinezhad A, Sayari A (2014) Oxidative degradation of silica-supported polyethylenimine for CO_2 adsorption: insights into the nature of deactivated species. Phys Chem Chem Phys 16(4):1529–1535
38. Bali S, Chen TT, Chaikittisilp W, Jones CW (2013) Oxidative stability of amino polymer-alumina hybrid adsorbents for carbon dioxide capture. Energy Fuels 27(3):1547–1554
39. Wang DX, Wang XX, Song CS (2017) Comparative study of molecular basket sorbents consisting of polyallylamine and polyethylenimine functionalized SBA-15 for CO_2 capture from flue gas. ChemPhysChem 18(22):3163–3173
40. Qian Y, Delgado JDLP, Veneman R, Brilman DWF (2017) Stability of a benzyl amine based CO_2 capture adsorbent in view of regeneration strategies. Ind Eng Chem Res 56(12):3259–3269
41. Srikanth CS, Chuang SSC (2012) Spectroscopic investigation into oxidative degradation of silica-supported amine sorbents for CO_2 capture. Chemsuschem 5(8):1435–1442
42. Gebald C, Wurzbacher JA, Tingaut P, Steinfeld A (2013) Stability of amine-functionalized cellulose during temperature-vacuum-swing cycling for CO_2 capture from air. Environ Sci Technol 47(17):10063–10070
43. Calleja G, Sanz R, Arencibia A, Sanz-Perez ES (2011) Influence of drying conditions on amine-functionalized SBA-15 as adsorbent of CO_2. Top Catal 54(1–4):135–145
44. Fan YF, Rezaei F, Labreche Y, Lively RP, Koros WJ, Jones CW (2015) Stability of amine-based hollow fiber CO_2 adsorbents in the presence of NO and SO_2. Fuel 160:153–164
45. Wu DZ, Sun CH, Dutta PK, Ho WSW (2017) SO_2 interference on separation performance of amine-containing facilitated transport membranes for CO_2 capture from flue gas. J Membr Sci 534:33–45
46. Rezaei F, Jones CW (2013) Stability of supported amine adsorbents to SO_2 and NO_x in postcombustion CO2 capture 1. Single-component adsorption. Ind. Eng. Chem. Res. 52(34):12192–12201
47. Wang P, Guo YF, Zhao CW, Yan JJ, Lu P (2017) Biomass derived wood ash with amine modification for post-combustion CO_2 capture. Appl Energy 201:34–44
48. Rezaei F, Jones CW (2014) Stability of supported amine adsorbents to SO_2 and NO_x in postcombustion CO_2 capture .2. Multicomponent adsorption. Ind. Eng. Chem. Res. 53(30):12103–12110
49. Liu Q, Xiong BT, Shi JJ, Tao MN, He Y, Shi Y (2014) Enhanced tolerance to flue gas contaminants on carbon dioxide capture using amine-functionalized multiwalled carbon nanotubes. Energy Fuels 28(10):6494–6501
50. Wang M, Yao LW, Wang JT, Zhang ZX, Qiao WM, Long DH, Ling LC (2016) Adsorption and regeneration study of polyethylenimine-impregnated millimeter-sized mesoporous carbon spheres for post-combustion CO_2 capture. Appl Energy 168:282–290

51. Chen XJ, Jiang JG, Yan F, Tian SC, Li KM (2014) A novel low temperature vapor phase hydrolysis method for the production of nano-structured silica materials using silicon tetrachloride. Rsc Adv 4(17):8703–8710
52. Srikanth CS, Chuang SSC (2013) Infrared study of strongly and weakly adsorbed CO_2 on fresh and oxidatively degraded amine sorbents. J Phys Chem C 117(18):9196–9205
53. Sayari A, Belmabkhout Y, Da'na E (2012) CO_2 deactivation of supported amines: does the nature of amine matter? Langmuir 28(9):4241–4247
54. Heydari-Gorji A, Sayari A (2012) Thermal, oxidative, and co_2-induced degradation of supported polyethylenimine adsorbents. Ind Eng Chem Res 51(19):6887–6894
55. Sayari A, Heydari-Gorji A, Yang Y (2012) CO_2-Induced degradation of amine-containing adsorbents: reaction products and pathways. J Am Chem Soc 134(33):13834–13842
56. Wilfong WC, Srikanth CS, Chuang SSC (2014) In situ ATR and DRIFTS studies of the nature of adsorbed CO_2 on tetraethylenepentamine films. ACS Appl Mater Interfaces 6(16):13617–13626
57. Sayari A, Belmabkhout Y (2010) Stabilization of amine-containing CO_2 adsorbents: dramatic effect of water vapor. J Am Chem Soc 132(18):6312–6314
58. Wei L, Gao Z, Wang Y (2017) Integrated two-stage adsorption for selective removal of CO_2 and SO_2 by amine-functionalized SBA-15. Asia-Pac J Chem Eng 12(4):660–670
59. Kim C, Cho HS, Chang S, Cho SJ, Choi M (2016) An ethylenediamine-grafted Y zeolite: a highly regenerable carbon dioxide adsorbent via temperature swing adsorption without urea formation. Energ Environ Sci 9(5):1803–1811
60. Lakard S, Herlem G, Lakard B, Fahys B (2004) Theoretical study of the vibrational spectra of polyethylenimine and polypropylenimine. J Mol Struc-Theochem 685(1–3):83–87
61. Hiyoshi N, Yogo K, Yashima T (2005) Adsorption characteristics of carbon dioxide on organically functionalized SBA-15. Micropor Mesopor Mat 84(1–3):357–365
62. Okabayashi H, Shimizu I, Nishio E, O'Connor CJ (1997) Diffuse reflectance infrared Fourier transform spectral study of the interaction of 3-aminopropyltriethoxysilane on silica gel. Behavior of amino groups on the surface. Colloid Polym Sci 275(8):744–753
63. Bio-Rad Laboratories, Inc., Informatics Division, The Sadtler Handbook of Infrared Spectra.
64. Wilfong WC, Chuang SSC (2014) Probing the adsorption/desorption of CO_2 on amine sorbents by transient infrared studies of adsorbed CO_2 and C_6H_6. Ind Eng Chem Res 53(11):4224–4231
65. Knofel C, Martin C, Hornebecq V, Llewellyn PL (2009) Study of carbon dioxide adsorption on mesoporous aminopropylsilane-functionalized silica and titania combining microcalorimetry and in situ infrared spectroscopy. J Phys Chem C 113(52):21726–21734
66. Wankhade PM, Gambhire AB, Muley GG (2016) Influence of urea doping on optical, thermal, mechanical and electrical properties of L-arginine phosphate monohydrate crystals for NLO applications. Optik 127(6):3322–3328
67. Tailor R, Abboud M, Sayari A (2014) Supported polytertiary amines: highly efficient and selective SO_2 adsorbents. Environ Sci Technol 48(3):2025–2034
68. Tailor R, Ahmadalinezhad A, Sayari A (2014) Selective removal of SO_2 over tertiary amine-containing materials. Chem Eng J 240:462–468
69. Diaf A, Garcia JL, Beckman EJ (1994) Thermally reversible polymeric sorbents for acid gases—CO_2, SO_2, and NO_x. J Appl Polym Sci 53(7):857–875
70. Botheju D, Glarborg P, Tokheim LA (2012) NO_x reduction using amine reclaimer wastes (ARW) generated in post combustion CO_2 capture. Int J Greenh Gas Con 10:33–45
71. Drago RS, Paulik FE (1960) The reaction of nitrogen (II) oxide with diethylamine. J Am Chem Soc 82(1):96–98
72. Diaf A, Beckman EJ (1995) Thermally reversible polymeric sorbents for acid gases, IV. affinity tuning for the selective dry sorption of NOx. React Polym 25(1):89–96
73. Dai N, Shah AD, Hu LH, Plewa MJ, McKague B, Mitch WA (2012) Measurement of nitrosamine and nitramine formation from no reactions with amines during amine-based carbon dioxide capture for postcombustion carbon sequestration. Environ Sci Technol 46(17):9793–9801